THE JOURNAL OF PHYSICAL CHEMISTRY C

Article

pubs.acs.org/JPCC

First-Principles Study of Redox End Members in Lithium–Sulfur Batteries

Haesun Park,[†] Hyun Seung Koh,[†] and Donald J. Siegel*[,†,‡,§,∥]

[†]Mechanical Engineering Department, [‡]Applied Physics Program, [§]Michigan Energy Institute, and [∥]Joint Center for Energy Storage Research, University of Michigan, Ann Arbor, Michigan 48109-2125, United States

Supporting Information

ABSTRACT: The properties of the solid-phase redox end members, α-S, β-S, Li_2S, and Li_2S_2, are expected to strongly influence the performance of lithium–sulfur batteries. Nevertheless, the fundamental thermodynamic and electronic properties of these phases remain poorly understood. From a computational standpoint, the absence of these data can be explained by the omission of long-ranged van der Waals interactions in conventional density functionals; these interactions are essential for describing the molecular-crystal nature of S-based compounds. Here we apply van der Waals augmented density functional theory (vdW-DF), quasi-particle methods (G_0W_0), and continuum solvation techniques to predict several structural, thermodynamic, spectroscopic, electronic, and surface characteristics of these phases. The stability of the α allotrope of sulfur at low temperatures is confirmed by calculating the sulfur phase diagram. Similarly, the stability of lithium persulfide, Li_2S_2, a compound whose presence may limit capacity, was assessed by comparing the energies of several hypothetical A_2B_2 crystal structures. In all cases Li_2S_2 is predicted to be unstable with respect to a two-phase mixture of Li_2S and α-S, suggesting that Li_2S_2 is a metastable phase. Regarding surface properties, the stable surfaces and equilibrium crystallite shapes of Li_2S and α-S were predicted in the presence and absence of a continuum solvation field intended to mimic the effect of a dimethoxyethane (DME)-based electrolyte. In the case of Li_2S, the equilibrium crystallites are comprised entirely of stoichiometric (111) surfaces, while for α-S a complex mixture of several facets is predicted. Finally, G_0W_0 calculations reveal that all of α-S, β-S, Li_2S, and Li_2S_2 are insulators with band gaps greater than 2.5 eV.

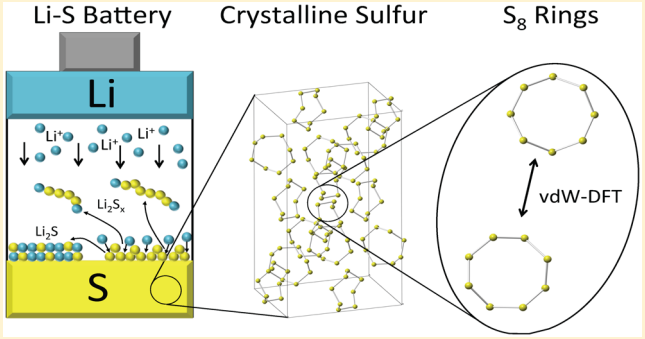

INTRODUCTION

Batteries based on lithium-ion chemistries have dramatically altered the energy storage landscape and in so doing have enabled a variety of new technologies such as portable electric devices.[1−8] Despite the higher energy density of Li-ion systems (~350 Wh/kg[1−7] theoretically and ~120 Wh/kg[9] at the system level) compared to earlier approaches based on nickel–metal-hydride or lead–acid systems, further gains in capacity are highly desirable for emerging applications such as in vehicle electrification.[1−7,9]

Lithium–sulfur (Li–S) batteries present a promising alternative to the Li-ion chemistry due to their high theoretical specific energy (~2200 Wh/kg),[2,7] and potential for low cost.[10] Recent cell designs involving nanostructured cathodes have improved cyclability and sparked renewed interest in sulfur-based systems.[10−14] Nevertheless, several performance gaps should be addressed before these systems become commercially viable, such as capacity fade[15] arising from the so-called "polysulfide shuttle" effect and the presumably insulating nature of solid-state redox end members consisting of sulfur and metal sulfides.[11] Understanding the properties of these compounds will foster the development of rational strategies that can overcome the aforementioned limitations.

One issue of both fundamental and practical importance is the relative stability of Li–S redox end members. For example, lithium persulfide, Li_2S_2, has been proposed as an insoluble discharge product in Li–S batteries.[20,26,27] The formation of Li_2S_2 would be undesirable, as it has been suggested to limit capacity.[15−17] However, as Li_2S_2 does not appear in the Li–S phase diagram,[18] its presence as a discharge phase remains a matter of debate. A recent study based on X-ray absorption near-edge spectroscopy (XANES)[19] found no evidence for the presence of Li_2S_2 during battery operation. Likewise, Hagen et al. employed Raman spectroscopy to characterize polysulfide formation in the Li–S system but was unable to directly identify Li_2S_2.[20]

In a similar vein, the presence of higher-temperature allotropes of sulfur has been suggested to impact the longevity of Li–S batteries. Recent experiments employing encapsulated sulfur or carbon fiber–sulfur composite cathodes[18,26] have observed the presence of β-sulfur, a monoclinic phase which in bulk form has been reported to be stable at temperatures above

Received: December 31, 2014
Revised: February 6, 2015
Published: February 9, 2015

DOI: 10.1021/jp513023v
J. Phys. Chem. C 2015, 119, 4675−4683

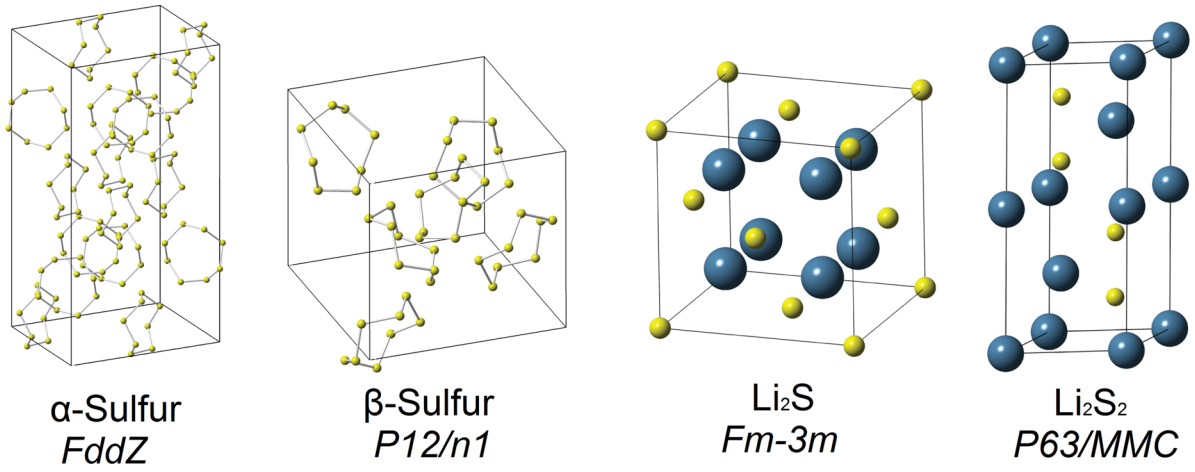

Figure 1. Crystal structures and respective space groups for α-sulfur, β-sulfur, Li_2S, and the lowest-energy structure for Li_2S_2. Blue and yellow spheres represent lithium and sulfur atoms, respectively.

approximately 95 °C.[21] However, these measurements were performed using cells cycled at room temperature[10,16] and reported reduced capacity fade. It was therefore suggested that the formation of β-sulfur could improve the cyclability, although the mechanism by which this could occur is unclear.

Another issue which can impact battery performance is the surface properties (i.e., composition and structure) of the redox end members.[22] The surfaces of these phases are expected to play a critical role in both electrochemical and chemical processes occurring in the cathode of Li−S batteries. For example, discharge[23] of a Li−S cell is believed to occur via the formation of soluble polysulfides according to the sequence:[2,14] $S_8 \rightarrow Li_2S_8 \rightarrow Li_2S_6 \rightarrow Li_2S_4 \rightarrow Li_2S_2 \rightarrow Li_2S$. From the standpoint of electrochemistry, charge transfer to/from these species is likely to to occur at surfaces of the solid-phase redox end members. From a chemical standpoint, surfaces are also likely to be the location for processes such as disproportionation, nucleation, and growth. The importance of surface phenomena also extends to approaches involving sulfur cathodes preloaded with Li_2S particles.[24−26] In this regard, a necessary step in understanding the reaction sequence associated with cycling of a Li−S cell is to determine the stable surface terminations of solid phases present in the sulfur cathode.

Transport phenomena are also expected to impact the performance of Li−S batteries. For example, sulfides are believed to be electrically insulating,[27] and electrical passivation by a resistive discharge product has been proposed as a major obstacle to achieving both high capacity and efficient charging in related precipitation−dissolution systems such as the Li−O_2 battery.[28,29] In the case of Li−S batteries, a thick film of sulfur or Li_2S could limit charge transfer across the film, leading to early cell death during discharge and high overpotentials during charging.[26] Consequently, the charge transport properties of redox end members play an important role in battery performance. Nonetheless the band gap and conductivity of these phases have received little attention.

In the present study first-principles calculations are used to close some of the knowledge gaps mentioned above by predicting key thermodynamic and electronic properties of several solid-phase redox end members present in lithium−sulfur batteries. The phases examined include: Li, (hypothetical) Li_2S_2, Li_2S, α-sulfur, and β-sulfur. A variety of computational methods were employed, including: density functional theory (DFT) with semilocal functionals, van der Waals augmented DFT (vdW-DF), quasi-particle methods (G_0W_0), and continuum solvation techniques. First, optimized crystal structures were characterized in a comparative fashion using multiple van der Waals-aware density functionals. The vdW-DF method using the optB88 functional for electron exchange was found to yield the best agreement with experimental lattice constants and bulk moduli. The stability of the α allotrope of sulfur at low temperatures was confirmed by revisiting the sulfur phase diagram. Similarly, the stability of lithium persulfide, Li_2S_2, was assessed by comparing the energies of several hypothetical A_2B_2 crystal structures. We find that Li_2S_2 is unstable with respect to a two-phase mixture of Li_2S and α-S, suggesting that Li_2S_2 is a metastable phase. Regarding surface properties, the stable surfaces and equilibrium crystallite shapes of Li_2S and α-S were predicted in the presence and absence of a continuum solvation field intended to mimic the presence of the common electrolyte solvent, dimethoxyethane (DME). In the case of Li_2S, the equilibrium crystallites are comprised entirely of stoichiometric (111) surfaces, while for α-S a complex mixture of several facets are predicted. Finally, G_0W_0 calculations reveal that all of α-S, β-S, Li_2S, and Li_2S_2 are insulators with band gaps greater than 2.5 eV.

METHODOLOGY

First-principles calculations were performed using the Vienna *ab initio* simulation package (VASP).[30] Five compounds were considered: BCC Li (2 atoms in the unit cell), Li_2S (3 atoms), Li_2S_2 (8 atoms), α-sulfur (128 atoms), and β-sulfur (48 atoms). Figure 1 displays the crystal structures and space groups of α-sulfur, β-sulfur, Li_2S, and Li_2S_2, the latter using the crystal structure that exhibits the lowest energy out of several possibilities (described below). Projector-augmented wave (PAW)[31,32] potentials were used to describe core−valence electron interactions. Valence states of 2s were used for lithium and 3s3p for sulfur. The plane-wave cutoff energy was set to 450 eV; the Monkhorst−Pack[33] scheme for k-point sampling was used in combination with k-point meshes of: 12 × 12 × 12 (Li), 4 × 4 × 4 (Li_2S), 7 × 7 × 7 (Li_2S_2), 2 × 2 × 2 (α-S), and 2 × 2 × 2 (β-S). Two methods were used to treat exchange and correlation: (i) the Perdew−Burke−Ernzerhof (PBE) general-

DOI: 10.1021/jp513023v
J. Phys. Chem. C 2015, 119, 4675−4683

ized gradient approximation (GGA)[34] and (ii) van der Waals-augmented density functional theory (vdW-DF).[35] Including van der Waals interactions is essential for describing the behavior of sulfur, as the crystal structure of both α and β allotropes consists of discrete, covalently bonded S_8 molecular units ("cycloocta") that interact through dispersion forces. Five different vdW-DF methods were tested: these include the so-called vdW-DF1 methods having exchange functionals based on revPBE,[35] optPBE,[36] optB88,[37] optB86b,[37] and also the vdW-DF2[38] method. Equilibrium cell volumes were determined by fitting energy−volume data to the Murnaghan equation of state.[39] Atom positions were relaxed to a force tolerance of 0.01 eV/Å.

As previously mentioned, the existence of a persulfide phase, Li_2S_2, during discharge of a Li−S battery remains an open question. Such a phase does not appear in the equilibrium Li−S phase diagram, and its crystal structure is unknown. To examine the stability of a hypothetical Li_2S_2 phase we generated several candidate Li_2S_2 crystal structures using various A_2B_2 phases as structural templates. Here A represents an alkali metal (Li, Na, K, Rb), and B is a chalcogenide (O, S, Se). Seven structures were investigated by replacing A sites with Li and B sites with S. The template compounds included: Li_2O_2, Na_2S_2, K_2S_2, Na_2O_2, K_2O_2, Na_2Se_2, and Rb_2S_2. In all cases the unit cells (volume, shape, and atom positions) were relaxed using vdW-aware DFT.

Thermodynamic properties were evaluated within the harmonic approximation.[27] Vibrational frequencies ω_i were obtained using the direct method.[40] Vibrational contributions to the enthalpy (H_{vib}) and entropy (S_{vib}) are given by[27]

$$H_{vib}(T) = \sum_{i}^{3N-3} \frac{1}{2}\hbar\omega_i + \hbar\omega_i \left[\exp\left(\frac{\hbar\omega_i}{k_B T}\right) - 1\right]^{-1} \quad (1)$$

$$S_{vib}(T) = \sum_{i}^{3N-3} \frac{\hbar\omega_i/k_B T}{\exp(\hbar\omega_i/k_B T)} - \ln\left[1 - \exp\left(\frac{-\hbar\omega_i}{k_B T}\right)\right] \quad (2)$$

where $\hbar$ is Planck's constant divided by 2π; k_B is the Boltzmann factor; and N refers to the number of atoms in the supercell. The enthalpy and Gibbs free energy are expressed as

$$H(T) = E + H_{vib}(T) \quad (3)$$

$$G(T) = H(T) - S_{vib}(T)T \quad (4)$$

where E is the static (0 K) energy of a compound in its ground state.

To estimate electronic properties, the Heyd−Scuseri−Ernzerhof (HSE06) hybrid functional[41] and the non-self-consistent quasi particle G_0W_0 method[42] were used. In the case of G_0W_0 calculations, vdW-DF wave functions from an earlier self-consistent calculation were used as input. A γ-point-centered sampling scheme with $1 \times 1 \times 1$ (α, β-S), $4 \times 4 \times 4$ (Li_2S), and $7 \times 7 \times 7$ (Li_2S_2) k-point meshes was used. The Gaussian smearing method was applied to obtain the density of states (DOS); the band gap was estimated using energy differences between the lowest occupied and highest unoccupied eigenvalues.

The surface energies of 38 distinct surfaces were evaluated. These included 31 Li_2S surfaces of varying stoichiometry[43] with Miller indices (100), (110), and (111). Each surface slab consisted of at least 9 Li/S planes; approximately 20 Å of vacuum was included in each surface supercell. For Li_2S surfaces, comparisons were made using the GGA and vdW-DF (optB88) functionals. In addition, seven sulfur surfaces were considered, with indices of (100), (010), (001), (011), (110), and (111). These surfaces were comprised of at least three layers of cycloocta rings and were constructed such that no S_8 rings were broken when the surface was cleaved. For sulfur surfaces only the vdW-DF method was used. The Monkhorst−Pack scheme was used for both Li_2S and sulfur surfaces with $4 \times 4 \times 1$ and $1 \times 1 \times 1$ k-point meshes, respectively.

The energies of Li_2S and S surfaces are given by

$$\gamma_{Li_2S} = \frac{1}{2A}(G^{slab}_{Li_2S} - N_{Li}\mu_{Li} - N_S\mu_S) \quad (5)$$

$$\gamma_S = \frac{1}{2A}(G^{slab}_{S} - N_S\mu_S) \quad (6)$$

where G^{slab} is the energy of the surface slab; N_i is the number of atoms of type i in the slab; and μ_i is the corresponding chemical potential. In the case of the Li_2S surface, the surface energy can be written in terms of the energy per formula unit of bulk Li_2S, g_{Li2S}, and the chemical potential of sulfur

$$\gamma_{Li_2S} = \frac{1}{2A}\left[G^{slab}_{Li_2S} - \frac{1}{2}N_{Li}g^{bulk}_{Li_2S} + \left(\frac{1}{2}N_{Li} - N_S\right)\mu_S\right] \quad (7)$$

As the chemical potential of sulfur is not precisely known, surface energies were evaluated for a range of μ_S given by $E(Li_2S) - 2\,\mu_{Li}(\text{BCC Li}) \le \mu_S \le \mu_S(\alpha\text{-S})$. Here, $E(Li_2S)$ is the total energy of a Li_2S formula unit; μ_{Li}(BCC Li) is the energy per atom of BCC Li; and $\mu_S(\alpha\text{-S})$ refers to the same for an atom of α-S.

Cycling of a Li−S battery should result in the repeated nucleation and growth of solid-phase sulfur (charging) and Li−S particles (discharging). As these processes occur in the presence of a liquid electrolyte, the relevant "surface" energies are not solid/vacuum surface energies—as is typically assumed in atomistic studies—but rather solid electrode/liquid electrolyte interface energies.

To explore the impact of solvation on surface energies, comparisons were made with and without a continuum solvation field (VASPsol).[51,52] In these calculations the dielectric constant was set to that of dimethoxyethane (DME),[53] 7.55, as common electrolytes in Li−S batteries employ solvents based on DME[11] or mixtures of DME and dioxolane.[10,19] (The dielectric constant of dioxolane is similar to that of DME, 7.13.)

RESULTS

Structure Analysis. Low-energy structures of each redox end member were evaluated in a comparative fashion using the GGA and five different vdW-DF methods. Turning first to the high-temperature β-sulfur phase, Figure S1 (Supporting Information) plots the total energy of the β-S unit cell as a function of cell volume. In contrast to the other functionals, which show a clear minimum in the energy vs volume data, the curves calculated with the GGA and the revPBE-based vdW-DF1 functional monotonically decrease as volume increases. Such behavior might be expected from the GGA, where the neglect of vdW interactions between cycloocto rings is a known omission. However, in the case of vdW-DF1, vdW contributions are explicitly accounted for; hence, the poor representation of energy−volume behavior is surprising. For this reason, the GGA and revPBE-based vdW-DF1 functionals were not used in subsequent structure calculations on S-based systems.

DOI: 10.1021/jp513023v
J. Phys. Chem. C 2015, 119, 4675−4683

Table 1. Calculated Bulk Modulus, Lattice Parameters, and Unit Cell Volume of Li and Li−S Redox End Members Using the optB88-vdW Functional

			lattice parameters				
	functional	bulk modulus (GPa)	*a* (Å)	*b* (Å)	*c* (Å)	angle (deg)	volume (Å^3)
Li	optB88-vdW	13.8	3.45			90	40.9
	experiment	12.9[44]	3.48[45]			90	43.2
Li_2S	optB88-vdW	42.6	5.70			90	185.1
	experiment	45.7[46]	5.69[47]			90	184.2
α-S	optB88-vdW	11.3	10.33	12.76	24.45	90	3221
	experiment	14.5[48]	10.46[49]	12.87	24.49	90	3296
β-S	optB88-vdW	10.8	10.66	10.72	10.84	95.44	1232
	experiment	-	10.69[50]	10.72	10.81	95.75	1233

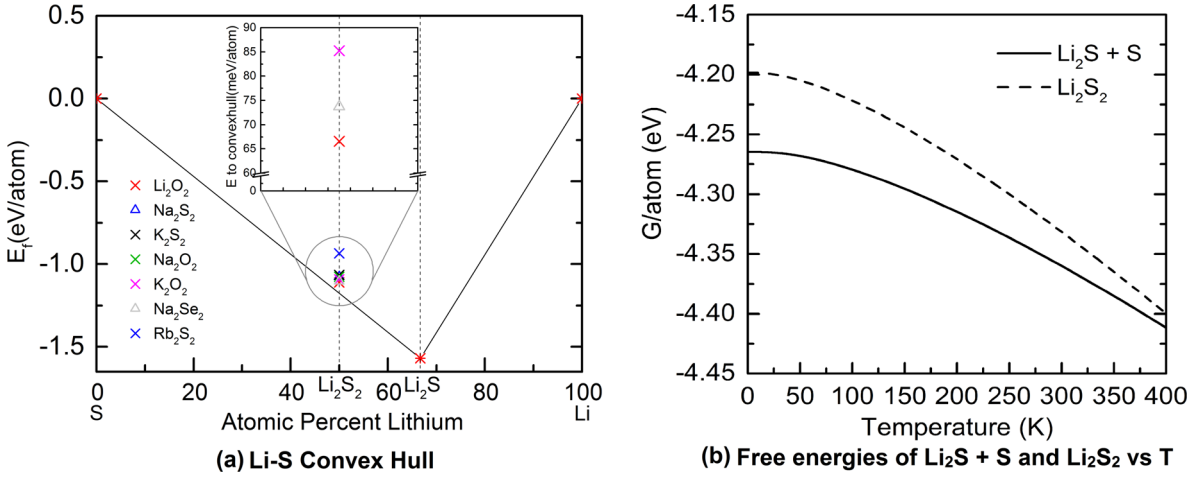

Figure 2. (a) Calculated convex hull for the Li−S system. The inset magnifies the energetic ordering of the different Li_2S_2 candidate phases above the hull. (b) Gibbs free energy of Li_2S + S vs Li_2S_2 as a function of temperature. Relaxed structures and vibrational contributions were calculated using the optB88-vdW functional, while total energies were evaluated using the vdW-DF2 functional.

Table 1 compares the calculated bulk modulus, lattice parameters, and cell volume of Li−S redox end members with experimental data. The calculated values are from the optB88-vdW functional, which comparison calculations (Table S1, Supporting Information) revealed performed the best for structural properties among three other functionals: optPBE-vdW, optB86b-vdW, and vdW-DF2. Typical deviations between theory and experiment were less than 1% for the optB88-vdW. The optB86b- and optPBE-based functionals have slightly larger deviations (1−2%), whereas vdW-DF2 exhibits a range of 1−3%.

Thermodynamic Properties. Figure 2a shows the convex hull for the Li−S system as a function of atomic percent lithium at 0 K. Among the various structure candidates considered for Li_2S_2, the one yielding the lowest energy was based on the hexagonal Li_2O_2 prototype (*P*63/*MMC* space group). This structure lies above the convex hull by approximately 67 meV/atom and should therefore be metastable with respect to a two-phase mixture of S and Li_2S. Of course, other hypothetical structures for Li_2S_2 are possible; however, identifying them will require a more extensive search (using genetic algorithms, etc.), which is beyond the scope of the present study. While such an effort might yield a structure whose energy is lower than the Li_2O_2 prototype identified here, the energy above the convex hull calculated for this structure, 67 meV, is sizable and in our judgement would be difficult to overcome with an alternative structure. Regarding the accuracy of this prediction, ref 54 reported that typical errors associated with DFT phase stability calculations involving oxides exhibited a standard deviation of 24 meV/atom. If the conclusions from oxides can be transferred to sulfides (to our knowledge a similar study on sulfides does not exist), then the energy above the hull for Li_2S_2 reported here safely exceeds the error threshold. The Li_2O_2 prototype for Li_2S_2 was used for calculations involving Li_2S_2 henceforth.

Figure 2b compares the Gibbs free energies of Li_2S_2 to the two-phase mixture, Li_2S + α-S, as a function of temperature. Free energies were evaluated by combining the static electronic energy from the vdW-DF2 functional with vibrational contributions obtained from the optB88-vdW. For the entire temperature range considered (0−400 K), we find that the two-phase mixture of Li_2S and S has lower free energy than Li_2S_2. As previously mentioned, Li_2S_2 has not been successfully synthesized and does not appear in experimental phase diagrams.[18] The calculated thermodynamic data in Figure 2 are consistent with these observations. To aid in the identification of Li_2S_2 during discharge of Li−S batteries, Figure S2 (Supporting Information) plots the calculated XRD pattern for Li_2S_2 and compares to that of Li_2S. Li_2S has major peaks around 27°, 31°, 45°, and 53°, which correspond well to experimental data.[19] On the other hand, the peaks of Li_2S_2 do not match data from recent experiments.[19,55]

Table 2 summarizes the calculated redox potentials, formation enthalpies (ΔH), and formation free energies (ΔG) for Li_2S and Li_2S_2 at room temperature (298 K). Comparisons are made between different functionals by

DOI: 10.1021/jp513023v
J. Phys. Chem. C 2015, 119, 4675−4683

Table 2. Calculated Cell Potential ($E^{T=298K}$), Formation Enthalpy ($\Delta H^{T=298K}$), and Gibbs Free Energy of Formation ($\Delta G^{T=298K}$) for Several vdW-DF Methods Compared with Experimental Data

		$E^{T=298K}$ (V)	$\Delta H^{T=298K}$ (eV)	$\Delta G^{T=298K}$ (eV)
Li_2S	optPBE	2.15	−4.35	−4.30
	optB88	2.20	−4.44	−4.40
	opt86b	2.10	−4.24	−4.19
	vdW-DF2	2.33	−4.70	−4.65
	Exp.	2.30[10]	−4.58[56]	-
Li_2S_2	optPBE	2.07	−4.10	−4.14
	optB88	2.13	−4.23	−4.27
	opt86b	2.04	−4.03	−4.07
	vdW-DF2	2.22	−4.40	−4.44
	Exp.	-	-	-

evaluating the static electronic energy with several vdW-DF methods. (Phonon frequencies were evaluated using the harmonic approximation and the optB88-vdW functional. We found that the optB88-vdW yields the expected number (3) of imaginary frequencies, whereas most of the other functionals did not.) The calculated ΔH values for Li_2S are in good agreement with experimental data, with an error range of 1−6%. The vdW-DF2 method yielded energies that were closest to experiment. For example, the calculated cell potential at 298 K was found to be similar to the experimental cell voltage at the upper plateau of the discharge curve.[10] To the best of our knowledge, experimental data for ΔG for Li_2S and Li_2S_2, and ΔH for Li_2S_2, have not been reported. The formation energy data presented in Table 2 are consistent with the thermodynamic analysis presented in Figure 2: Li_2S is predicted to have a more negative formation enthalpy/free energy than Li_2S_2 by ∼0.1 eV at room temperature, suggesting that Li_2S_2 generated during battery discharge should transform via a nonelectrochemical pathway to a mixture of Li_2S and S. The transformation of Li_2S_2 to Li_2S via the reaction $Li_2S_2 + 2Li \rightarrow 2Li_2S$ could also be limited in the event that the reaction is starved of Li.

Regarding the phase diagram for elemental sulfur, recent experiments[10] have correlated reduced capacity fade (due to limited polysulfide shuttling) in Li−S batteries with the formation of β sulfur in the cathode. In bulk S the α phase is observed to be the stable phase at low temperatures, with a transition to the β phase at temperatures ranging from room temperature to slightly above.[18,25] Figure 3 plots the free energy difference, $G(\alpha\text{-S}) - G(\beta\text{-S})$, between the α and β allotropes of sulfur as a function temperature. The present calculations reproduce the stability trends observed in experiments involving bulk sulfur but underpredict the α/β transition temperature, $T(\alpha \rightarrow \beta)$, by approximately 200 K. The reasonable agreement between the calculated and measured phase diagram suggests that the presence of β-S within a Li−sulfur battery cathode at temperatures below $T(\alpha \rightarrow \beta)$ is a consequence of slow kinetics or due to stabilizing (interfacial) interactions with the cathode support.

Electronic Structure. Figure 4 plots the density of states (DOS) for Li_2S and Li_2S_2 (panel a), as well as for α-sulfur and β-sulfur (panel b). Several different calculation methods were compared: optB88-vdW-DF, HSE06, and G_0W_0. In the case of G_0W_0 calculations, optB88-vdW-DF wave functions were used as input; we refer to this approach as vdW-DF+G_0W_0. The DOS reveals that all of the compounds considered exhibit a

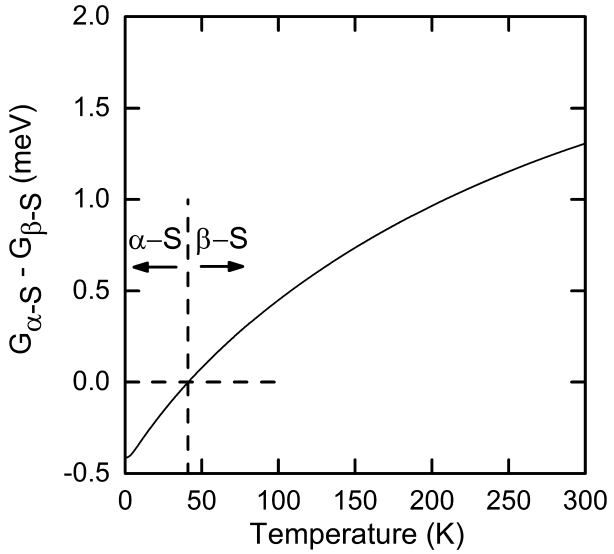

Figure 3. Calculated Gibbs free energy difference between α and β sulfur as a function of temperature.

sizable band gap. Furthermore, the DOS of the sulfur allotropes are quite similar in both shape and size of the gap. On the other hand the DOS of Li−S phases display some clear differences: for example, Li_2S_2 generally has a smaller gap than Li_2S, due to the presence of lower-lying states at the bottom of the conduction band.

Table 3 summarizes the calculated band gaps and makes comparisons with experimental data. (The apparent gaps in Figure 4 appear somewhat smaller than the tabulated gaps in Table 3 due to the use of smearing in plotting the DOS.) Due to its large unit cell size (128 atoms), G_0W_0 calculations were not performed for α-sulfur. However, its value can be estimated based on comparisons with β-sulfur. We note that the band gaps of α- and β-sulfur are similar for vdW-DF and HSE06 calculations, with the gap for the β phase being larger by 0.1−0.2 eV. Assuming this trend holds, we can estimate the band gap for α-sulfur at the G_0W_0 level to be ∼0.2 eV smaller than the corresponding value for β-sulfur, approximately 3.6 eV.

Table 3 shows that the calculated band gap increases in going from the vdW-DF functional, to HSE06, to G_0W_0. Such behavior is consistent with generally known trends.[41,57] G_0W_0 calculations based on GGA starting wave functions generally underestimate the experimental band gap.[57] In our calculations vdW-DF-based wave functions are used, which appear to result in an overestimate of the gap: in the case of the S allotropes the calculated gap of 3.6−3.76 eV at the G_0W_0 level is approximately 1 eV larger than the experimental values. This discrepancy could also be due to the molecular-crystal nature of sulfur.[58] We note that the temperature dependence of the sulfur band gap (≈2 meV/K)[58] is approximately 10 times higher than that of other semiconductors (∼0.1 meV/K).[59] Our calculation is conducted at 0 K, while the experimental values for the band gap are reported at 298 K[60] and 279 K,[58] respectively. Accounting for this temperature dependence, the calculated band gap of sulfur at 298 K ranges from 2.9 to 3.3 eV. This is in much better agreement with the measured values of 2.6 and 2.8 eV.

Regarding lithium sulfide, a prior study predicted the band gap of Li_2S to be 3.66 eV when using the GGA functional.[26] The band gap of 3.46 eV predicted here using vdW-DF is similar to that value. As expected,[41] the gap opens to 4.34 eV

DOI: 10.1021/jp513023v
J. Phys. Chem. C 2015, 119, 4675−4683

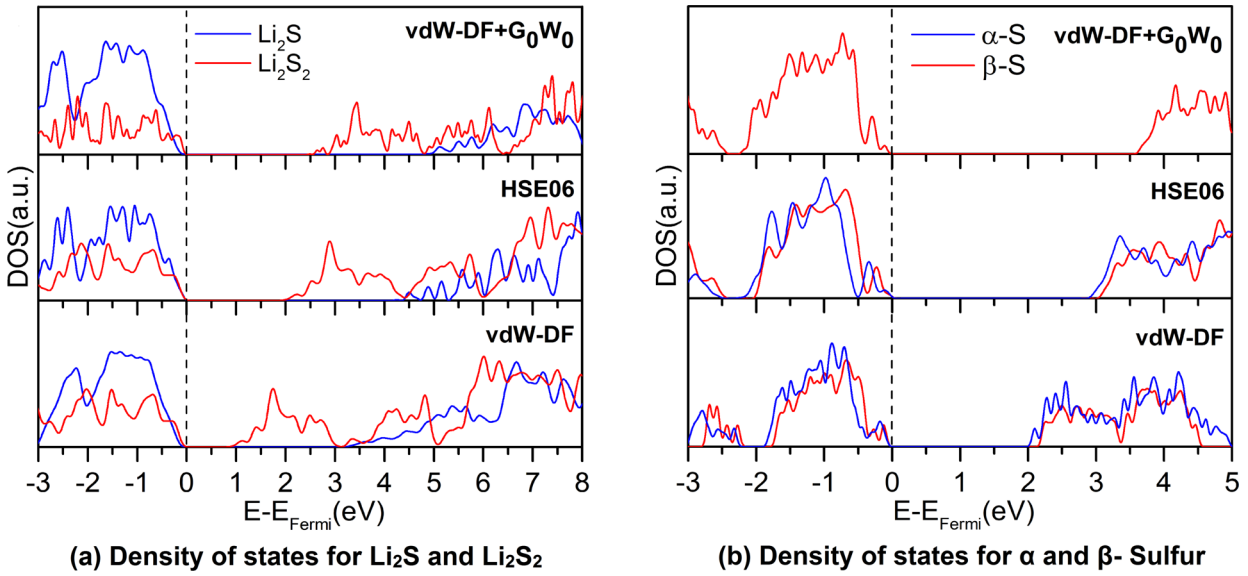

Figure 4. Density of states for (a) Li_2S and Li_2S_2 and (b) α- and β-sulfur calculated using vdW-DF, HSE06, and vdW-DF+G_0W_0.

Table 3. Calculated and Experimental Band Gap of α-, β-Sulfur, Li_2S, and Li_2S_2[a]

	band gap			
method type	α-sulfur	β-sulfur	Li_2S	Li_2S_2
vdW-DF	2.20	2.34	3.46	1.07
HSE06	3.01	3.20	4.34	1.98
vdW-DF+G_0W_0	-	3.76	5.10	2.58
GGA+G_0W_0	-	-	5.11	2.70
Exp.	2.79,[60] 2.61[58]	-	-	-

[a]The reported experimental band gaps were measured at near-ambient temperatures, while the calculations are performed at 0 K. Extrapolating the experimental data to zero K yields gaps in the range from 2.9 to 3.3 eV.

when using the HSE06 hybrid functional and is largest for the vdW-DF + G_0W_0, 5.10 eV. These gaps indicate that Li_2S is an electronic insulator, a fact which could limit battery performance if charge transport through Li_2S is needed during charge or discharge.[11] To the best of our knowledge, an experimental value for the Li_2S band gap has not been reported.

Surface Energy. Figure S3 (Supporting Information) shows the GGA free energies of 31 Li_2S surfaces as a function of sulfur chemical potential. The surfaces were selected from the low-index (100), (110), and (111) cleavage planes and take several different terminations into account. (Relaxed configurations of all Li_2S surfaces considered are shown in Figure S4 (Supporting Information).) We adopt a naming convention wherein surfaces are identified using their respective Miller indices followed by "Li", "S", or "stoichi". These identify the stoichiometry of the slab as being either lithium-rich, sulfur-rich, or stoichiometric, respectively. As previously described, the upper "S-rich" limit of the sulfur chemical potential—defined as zero for convenience—corresponds to the chemical potential of elemental sulfur.

Comparison calculations similar to those in Figure S3 (Supporting Information) were also performed using the optB88-based vdW-DF functional and by combining the GGA with solvation effects. Figure 5 summarizes these results across all three calculation methods—GGA (Figure 5a), vdW-DF (Figure 5b), and GGA with solvation (Figure 5c)—by plotting the lowest-energy terminations for each of the three

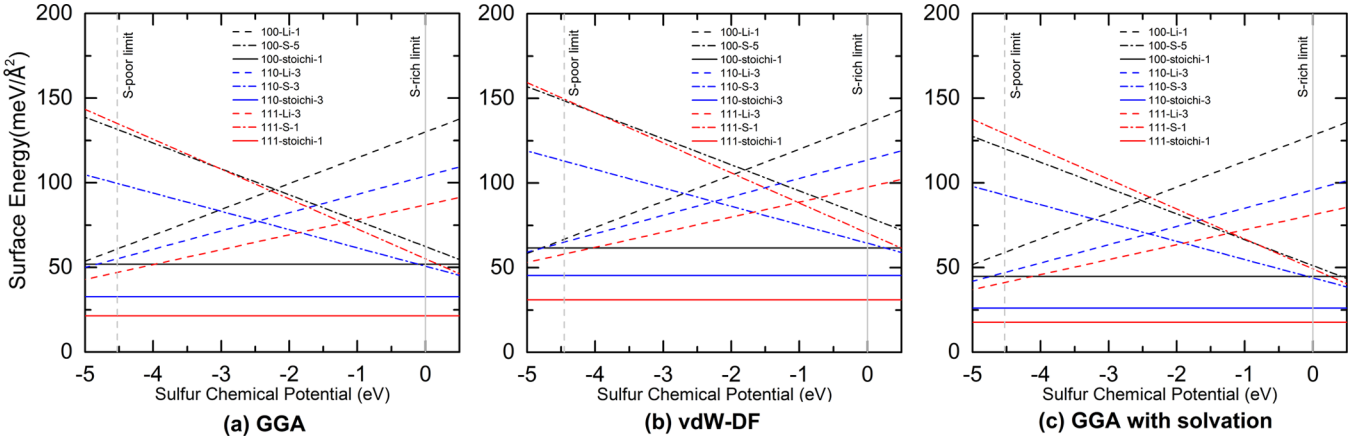

Figure 5. Free energies of Li_2S surfaces as a function of sulfur chemical potential and calculation method. (a) GGA, (b) vdW-DF, and (c) GGA + solvation. Vertical lines represent sulfur-poor and -rich limits to the S chemical potential. The three lowest-energy surfaces are plotted for each of the three surface normals considered: 100, 110, and 111.

DOI: 10.1021/jp513023v
J. Phys. Chem. C 2015, 119, 4675−4683

surface normals. All calculation methods agree that a stoichiometric termination of the (111) surface (i.e., the surface identified as "111-stoichi-1") has the lowest surface energy overall. Except at the extreme limits of the S chemical potential, stoichiometric surfaces are also predicted to be the most stable for (100) and (110) facets. These results agree well with a prior study of Li_2S surfaces that employed the GGA functional.[26]

Table 4 summarizes the calculated surface energies for the most stable termination of each (*hkl*) facet across the three

Table 4. Most Thermodynamically Stable Li_2S Surface for Each Facet ((100), (110), and (111)) and Its Respective Surface Energy, As a Function of Calculation Method (GGA, vdW-DF, and GGA + Solvation)

	surface free energy (meV/Å^2)		
surface name	GGA	vdW-DF	GGA + solvation
100-stoichi-1	52	61	45
110-stoichi-3	33	45	26
111-stoichi-1	21	31	18

different calculation methods. Compared to the GGA calculations, surface energies calculated with the vdW-DF are ~10 meV/Å^2 larger. On the other hand, inclusion of solvation effects results in a slight reduction in surface energies by 3−7 meV/ Å^2, as expected. Given that all three methods predict the same stable surface, we conclude that neither van der Waals contributions nor solvation effects have a significant impact on the termination of Li_2S surfaces.

Using the calculated surface energies as input, Figure 6 plots the equilibrium shape of a Li_2S crystallite using the Wulff

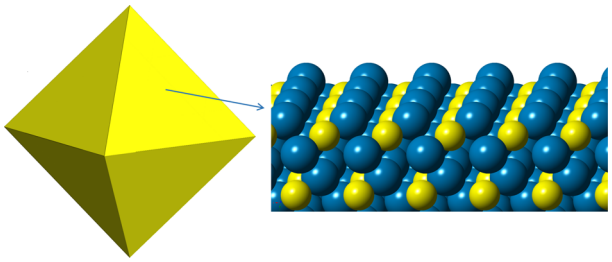

Figure 6. (Left) Equilibrium shape of a Li_2S crystallite based on the Wulff construction and calculated surface energies. (Right) Stoichiometric (111) surface which comprises all faces of the crystallite; blue and yellow spheres represent lithium and sulfur atoms, respectively.

construction.[61] All calculations methods—GGA, vdW-DF, and GGA + solvation—yield the same crystallite morphology, an octahedron whose surface is completely comprised of stoichiometric (111) surfaces. Such a shape is consistent both with a prior computational study of Li_2S surfaces[26] and with scanning electron microscopy (SEM) images of Li_2S crystallites.[62,63]

Figure S5 (Supporting Information) shows the layer-projected density of states (DOS) for the 111-stoichiometric surface of Li_2S, calculated using the vdW-DF method. The DOS for each layer shows the presence of a significant gap separating occupied and unoccupied states, indicative of insulating behavior. This behavior is similar to that previously discussed for bulk Li_2S in Figure 4a. We therefore conclude that the surface electronic structure of Li_2S does not significantly differ from that of the bulk.

Regarding α-sulfur, surface energies were calculated for seven distinct surfaces (cleaved along six <*hkl* > directions) with the vdW-DF with and without solvation effects. Surface models were constructed without cleaving the cycloocta sulfur rings; we presume that surfaces containing broken S−S bonds would exhibit in much higher energies. Relaxed geometries for all sulfur surfaces considered are shown in Figure S4 (Supporting Information). Table 5 summarizes the calculated surface

Table 5. Calculated Surface Energies of α-S Surfaces and Their Respective Area Fraction of the Equilibrium Crystallite Shape

	surface energy (meV/Å^2)		surface area fraction (%)	
surface	vdW-DF	VASPsol	vdW-DF	VASPsol
001	12	11	30.3	25.0
010	16	13	3.6	1.5
100	11	11	23.2	14.5
011	16	13	8.8	11.8
110	13	10	34.2	47.1
111	17	14	0.0	0.0

energies for the most stable terminations. In contrast to the surfaces of Li_2S, where only one low-energy termination (stoichiometric 111) dominated, in the case of S several surfaces have energies in a tightly clustered range of 10−14 meV/Å^2 (including solvation effects). (Similar behavior holds without solvation.) Consequently, the resulting Wulff plot (Figure 7a: without solvation effects; Figure 7b: including

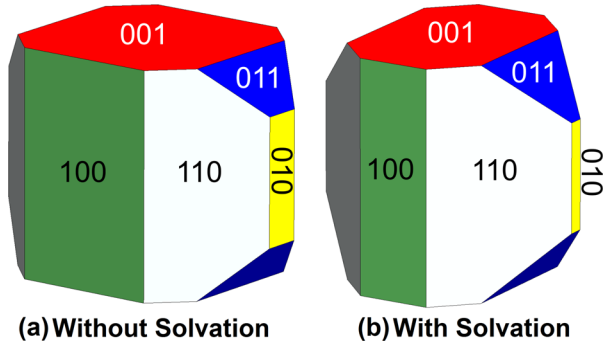

Figure 7. Equilibrium shape of α-S crystallites based on the Wulff construction and surface energies calculated using the optB88 vdW-DF functional. (a) Neglecting solvation effects. (b) Including solvation effects. Red, yellow, green, blue, and white areas represent (001), (010), (100), (011), and (110) facets, respectively.

solvation) is more complex, with five out of the six surfaces contributing to the area of the equilibrium crystallite (Table 5). For both calculation methods (110) facets cover the largest fraction of the crystallite surface area. The presence or absence of solvation effects has a minor effect on the equilibrium crystallite shape. The calculated crystallite shapes are in reasonable agreement with experimental electron microscopy images, which exhibit a hexagonal profile when viewed along a 001 direction.[25]

CONCLUSION

Understanding the properties of the solid-phase redox end members, α-S, β-S, Li_2S, and Li_2S_2, is an important step in improving the performance of lithium−sulfur batteries. Despite the growing importance of electrical energy storage devices, the

DOI: 10.1021/jp513023v
J. Phys. Chem. C 2015, 119, 4675−4683

fundamental thermodynamic and electronic properties of these phases remain poorly understood. In the present study several computational techniques—van der Waals augmented density functional theory (vdW-DF), quasi-particle methods (G_0W_0), and continuum solvation techniques—are employed to predict key structural, thermodynamic, spectroscopic, electronic, and surface characteristics of these phases.

The stability of the α allotrope of sulfur at low temperatures was confirmed by revisiting the sulfur-phase diagram. Likewise, the stability of lithium persulfide, Li_2S_2—a phase whose presence during discharge is believed limit capacity—was assessed by comparing the energies of several hypothetical A_2B_2 crystal structures. In all cases Li_2S_2 was predicted to be unstable with respect to decomposition into a two-phase mixture of Li_2S and α-S, suggesting that Li_2S_2 is a metastable phase.

Regarding surface properties, the stable surfaces and equilibrium crystallite shapes of Li_2S and α-S were predicted in the presence and absence of a continuum solvation field intended to mimic the effect of a dimethoxyethane (DME)-based electrolyte. In the case of Li_2S, equilibrium crystallites are comprised entirely of stoichiometric (111) surfaces, while for α-S a complex mixture of several facets is predicted.

Finally, G_0W_0 calculations reveal that all of α-S, β-S, Li_2S, and Li_2S_2 are insulators with band gaps greater than 2.5 eV.

The properties revealed by this study provide a "baseline understanding" of the solid-phase redox end members in Li−S batteries. We anticipate that this data will be of value in understanding pathways associated with charge and discharge reactions in these systems and foster development of approaches that move the Li−S chemistry closer to commercial viability.

■ ASSOCIATED CONTENT

Supporting Information

Calculated lattice constants of redox end members using different vdW-DF methods and their associated experimental values; total energy of the β-S unit cell as a function of cell volume using various methods; calculated X-ray diffraction patterns for Li_2S and Li_2S_2; calculated surface energies for Li_2S as a function of sulfur chemical potential, surface normal, and calculation method; relaxed structures of Li_2S and sulfur surfaces. This material is available free of charge via the Internet at http://pubs.acs.org.

■ AUTHOR INFORMATION

Corresponding Author

*E-mail: djsiege@umich.edu. Tel.: +1 (734) 764-4808.

Notes

The authors declare no competing financial interest.

■ ACKNOWLEDGMENTS

This work was supported as part of the Joint Center for Energy Storage Research, an Energy Innovation Hub funded by the U.S. Department of Energy, Office of Science, and Basic Energy Sciences. H.P. acknowledges support from the Kwanjeong Educational Foundation.

■ REFERENCES

(1) Whittingham, M. S. Lithium Batteries and Cathode Materials. *Chem. Rev.* **2004**, *104*, 4271−4302.
(2) Bruce, P. G.; Freunberger, S. A.; Hardwick, L. J.; Tarascon, J.-M. Li-O2 and Li-S batteries with high energy storage. *Nat. Mater.* **2012**, *11*, 19−29.
(3) Chiang, Y.-M. Building a Better Battery. *Science* **2010**, *330*, 1485−1486.
(4) Goodenough, J. B.; Park, K.-S. The Li-Ion Rechargeable Battery: A Perspective. *J. Am. Chem. Soc.* **2013**, *135*, 1167−1176.
(5) Kang, K.; Song, K.; Heo, H.; Yoo, S.; Kim, G.-S.; Lee, G.; Kang, Y.-M.; Jo, M.-H. Kinetics-driven high power Li-ion battery with a-Si/NiSix core-shell nanowire anodes. *Chem. Sci.* **2011**, *2*, 1090−1093.
(6) Kang, B.; Ceder, G. Battery materials for ultrafast charging and discharging. *Nature* **2009**, *458*, 190−193.
(7) Seh, Z. W.; Zhang, Q.; Li, W.; Zheng, G.; Yao, H.; Cui, Y. Stable cycling of lithium sulfide cathodes through strong affinity with a bifunctional binder. *Chem. Sci.* **2013**, *4*, 3673−3677.
(8) Lee, S. E.; Kim, H.-J.; Kim, H.; Park, J. H.; Choi, D.-G. Highly robust silicon nanowire/graphene core-shell electrodes without polymeric binders. *Nanoscale* **2013**, *5*, 8986−8991.
(9) Cairns, E. J.; Albertus, P. Batteries for Electric and Hybrid-Electric Vehicles. *Annu. Rev. Chem. Biomol. Eng.* **2010**, *1*, 299−320.
(10) Moon, S.; Jung, Y. H.; Jung, W. K.; Jung, D. S.; Choi, J. W.; Kim, D. K. Encapsulated Monoclinic Sulfur for Stable Cycling of Li−S Rechargeable Batteries. *Adv. Mater.* **2013**, *25*, 6547−6553.
(11) Ji, X.; Lee, K. T.; Nazar, L. F. A highly ordered nanostructured carbon-sulphur cathode for lithium-sulphur batteries. *Nat. Mater.* **2009**, *8*, 500−506.
(12) Fu, Y.; Su, Y.-S.; Manthiram, A. Sulfur−Carbon Nanocomposite Cathodes Improved by an Amphiphilic Block Copolymer for High-Rate Lithium−Sulfur Batteries. *ACS Appl. Mater. Interfaces* **2012**, *4*, 6046−6052.
(13) Xin, S.; Gu, L.; Zhao, N.-H.; Yin, Y.-X.; Zhou, L.-J.; Guo, Y.-G.; Wan, L.-J. Smaller Sulfur Molecules Promise Better Lithium−Sulfur Batteries. *J. Am. Chem. Soc.* **2012**, *134*, 18510−18513.
(14) Yang, Y.; Zheng, G.; Cui, Y. Nanostructured sulfur cathodes. *Chem. Soc. Rev.* **2013**, *42*, 3018−3032.
(15) Mikhaylik, Y. V.; Akridge, J. R. Polysulfide Shuttle Study in the Li/S Battery System. *J. Electrochem. Soc.* **2004**, *151*, A1969−A1976.
(16) Villevieille, C.; Novak, P. A metastable β-sulfur phase stabilized at room temperature during cycling of high efficiency carbon fibre-sulfur composites for Li-S batteries. *J. Mater. Chem. A* **2013**, *1*, 13089−13092.
(17) Yamin, H.; Gorenshtein, A.; Penciner, J.; Sternberg, Y.; Peled, E. Lithium Sulfur Battery: Oxidation/Reduction Mechanisms of Polysulfides in THF Solutions. *J. Electrochem. Soc.* **1988**, *135*, 1045−1048.
(18) Cunningham, P. T.; Johnson, S. A.; Cairns, E. J. Phase Equilibria in Lithium-Chalcogen Systems: II. Lithium-Sulfur. *J. Electrochem. Soc.* **1972**, *119*, 1448−1450.
(19) Cuisinier, M.; Cabelguen, P.-E.; Evers, S.; He, G.; Kolbeck, M.; Garsuch, A.; Bolin, T.; Balasubramanian, M.; Nazar, L. F. Sulfur Speciation in Li−S Batteries Determined by Operando X-ray Absorption Spectroscopy. *J. Phys. Chem. Lett.* **2013**, *4*, 3227−3232.
(20) Hagen, M.; Schiffels, P.; Hammer, M.; Dörfler, S.; Tübke, J.; Hoffmann, M. J.; Althues, H.; Kaskel, S. In-Situ Raman Investigation of Polysulfide Formation in Li-S Cells. *J. Electrochem. Soc.* **2013**, *160*, A1205−A1214.
(21) Okamoto, H. The Li-S (lithium-sulfur) system. *J. Phase Equilib.* **1995**, *16*, 94−97.
(22) Radin, M. D.; Rodriguez, J. F.; Tian, F.; Siegel, D. J. Lithium Peroxide Surfaces Are Metallic, While Lithium Oxide Surfaces Are Not. *J. Am. Chem. Soc.* **2011**, *134*, 1093−1103.
(23) Wang, L.; Zhang, T.; Yang, S.; Cheng, F.; Liang, J.; Chen, J. A quantum-chemical study on the discharge reaction mechanism of lithium-sulfur batteries. *J. Energy Chem.* **2013**, *22*, 72−77.
(24) Yang, Y.; McDowell, M. T.; Jackson, A.; Cha, J. J.; Hong, S. S.; Cui, Y. New Nanostructured Li2S/Silicon Rechargeable Battery with High Specific Energy. *Nano Lett.* **2010**, *10*, 1486−1491.
(25) Lin, Z.; Liu, Z.; Dudney, N. J.; Liang, C. Lithium Superionic Sulfide Cathode for All-Solid Lithium−Sulfur Batteries. *ACS Nano* **2013**, *7*, 2829−2833.
(26) Chen, Y.-X.; Kaghazchi, P. Metalization of Li_2S particle surfaces in Li-S batteries. *Nanoscale* **2014**, *6*, 13391−13395.

DOI: 10.1021/jp513023v
J. Phys. Chem. C 2015, 119, 4675−4683

(27) Wallace, D. C. *Thermodynamics of crystals*; Wiley: New York, 1972.
(28) Albertus, P.; Girishkumar, G.; McCloskey, B.; Sánchez-Carrera, R. S.; Kozinsky, B.; Christensen, J.; Luntz, A. C. Identifying Capacity Limitations in the Li/Oxygen Battery Using Experiments and Modeling. *J. Electrochem. Soc.* **2011**, *158*, A343−A351.
(29) Radin, M.; Tian, F.; Siegel, D. Electronic structure of Li_2O_2 {0001} surfaces. *J. Mater. Sci.* **2012**, *47*, 7564−7570.
(30) Kresse, G.; Furthmüller, J. Efficiency of ab-initio total energy calculations for metals and semiconductors using a plane-wave basis set. *Comput. Mater. Sci.* **1996**, *6*, 15−50.
(31) Kresse, G.; Joubert, D. From ultrasoft pseudopotentials to the projector augmented-wave method. *Phys. Rev. B* **1999**, *59*, 1758−1775.
(32) Blöchl, P. E. Projector augmented-wave method. *Phys. Rev. B* **1994**, *50*, 17953−17979.
(33) Monkhorst, H. J.; Pack, J. D. Special points for Brillouin-zone integrations. *Phys. Rev. B* **1976**, *13*, 5188−5192.
(34) Perdew, J. P.; Burke, K.; Ernzerhof, M. Generalized Gradient Approximation Made Simple. *Phys. Rev. Lett.* **1996**, *77*, 3865−3868.
(35) Dion, M.; Rydberg, H.; Schröder, E.; Langreth, D. C.; Lundqvist, B. I. Van der Waals Density Functional for General Geometries. *Phys. Rev. Lett.* **2004**, *92*, 246401.
(36) Klimeš, J.; Bowler, D. R.; Michaelides, A. Van der Waals density functionals applied to solids. *Phys. Rev. B* **2011**, *83*, 195131.
(37) Klimeš, J.; Bowler, D. R.; Michaelides, A. Chemical accuracy for the van der Waals density functional. *J. Phys.: Condens. Matter* **2010**, *22*, 022201.
(38) Lee, K.; Murray, E. D.; Kong, L.; Lundqvist, B. I.; Langreth, D. C. Higher-accuracy van der Waals density functional. *Phys. Rev. B* **2010**, *82*, 081101.
(39) Murnaghan, F. D. The Compressibility of Media under Extreme Pressures. *Proc. Natl. Acad. Sci. U.S.A.* **1944**, *30*, 244−247.
(40) Wei, S.; Chou, M. Y. *Ab initio* calculation of force constants and full phonon dispersions. *Phys. Rev. Lett.* **1992**, *69*, 2799−2802.
(41) Krukau, A. V.; Vydrov, O. A.; Izmaylov, A. F.; Scuseria, G. E. Influence of the exchange screening parameter on the performance of screened hybrid functionals. *J. Chem. Phys.* **2006**, *125*, 224106.
(42) Shishkin, M.; Kresse, G. Implementation and performance of the frequency-dependent *GW* method within the PAW framework. *Phys. Rev. B* **2006**, *74*, 035101.
(43) Reuter, K.; Scheffler, M. Composition, structure, and stability of RuO_2(110) as a function of oxygen pressure. *Phys. Rev. B* **2001**, *65*, 035406.
(44) Slotwinski, T.; Trivisonno, J. Temperature dependence of the elastic constants of single crystal lithium. *J. Phys. Chem. Solids* **1969**, *30*, 1276−1278.
(45) Berliner, R.; Fajen, O.; Smith, H. G.; Hitterman, R. L. Neutron powder-diffraction studies of lithium, sodium, and potassium metal. *Phys. Rev. B* **1989**, *40*, 12086−12097.
(46) Bührer, V. W.; Bill, U. H. Phononen-Dispersion in Na_2S. *Helv. Phys. Acta* **1977**, *50*, 431−438.
(47) Buehrer, W.; Altorfer, F.; Mesot, J.; Bill, H.; Carron, P.; Smith, H. G. Lattice dynamics and the diffuse phase transition of lithium sulphide investigated by coherent neutron scattering. *J. Phys.: Condens. Matter* **1991**, *3*, 1055.
(48) Luo, H.; Ruoff, A. X-ray-diffraction study of sulfur to 32 GPa: Amorphization at 25 GPa. *Phys. Rev. B* **1993**, *48*, 569−572.
(49) Rettig, S. J.; Trotter, J. Refinement of the structure of orthorhombic sulfur, α-S8. *Acta Crystallogr., Sect. C* **1987**, *43*, 2260−2262.
(50) David, W. I. F.; Ibberson, R. M.; Cox, S. F. J.; Wood, P. T. Order-disorder transition in monoclinic sulfur: a precise structural study by high-resolution neutron powder diffraction. *Acta Crystallogr., Sect. B* **2006**, *62*, 953−959.
(51) Mathew, K.; Sundararaman, R.; Letchworth-Weaver, K.; Arias, T. A.; Hennig, R. G. Implicit solvation model for density-functional study of nanocrystal surfaces and reaction pathways. *J. Chem. Phys.* **2014**, *140*, 084106.
(52) Fishman, M.; Zhuang, H. L.; Mathew, K.; Dirschka, W.; Hennig, R. G. Accuracy of exchange-correlation functionals and effect of solvation on the surface energy of copper. *Phys. Rev. B* **2013**, *87*, 245402.
(53) Wohlfarth, C., Dielectric constant of 1,2-dimethoxyethane. In *Supplement to IV/6*; Lechner, M. D., Ed.; Springer: Berlin Heidelberg, 2008; Vol. *17*, pp 263−268.
(54) Hautier, G.; Ong, S. P.; Jain, A.; Moore, C. J.; Ceder, G. Accuracy of density functional theory in predicting formation energies of ternary oxides from binary oxides and its implication on phase stability. *Phys. Rev. B* **2012**, *85*, 155208.
(55) Cañas, N. A.; Wolf, S.; Wagner, N.; Friedrich, K. A. In-situ X-ray diffraction studies of lithium−sulfur batteries. *J. Power Sources* **2013**, *226*, 313−319.
(56) Wangman, D. D.; Evans, Q. H.; Parker, V. B.; Schumm, R. H.; Halow, I.; Bailey, S. M.; Churney, K. L.; Nuttall, R. L., The NBS Tables of Chemical Thermodynamic Properties. Selected Values for Inorganic and C 1 and C 2 Organic Substances in SI Units. *J. Phys. Chem. Ref. Data* **1982**, *11* (Supplement No.2).
(57) Fuchs, F.; Furthmüller, J.; Bechstedt, F.; Shishkin, M.; Kresse, G. Quasiparticle band structure based on a generalized Kohn-Sham scheme. *Phys. Rev. B* **2007**, *76*, 115109.
(58) Abass, A. K.; Ahmad, N. H. Indirect band gap investigation of orthorhombic single crystals of sulfur. *J. Phys. Chem. Solids* **1986**, *47*, 143−145.
(59) Sze, S. M.; Ng, K. K. Appendix F Properties of Important Semiconductors. In *Physics of Semiconductor Devices*; John Wiley & Sons, Inc.: New York, 2006; pp 789−789.
(60) Liu, G.; Niu, P.; Yin, L.; Cheng, H.-M. α-Sulfur Crystals as a Visible-Light-Active Photocatalyst. *J. Am. Chem. Soc.* **2012**, *134*, 9070−9073.
(61) Wulff, G. On the question of the rate of growth and dissolution of crystal surfaces. *Z. Krystallogr. Mineral.* **1901**, *34*, 449.
(62) Nagao, M.; Hayashi, A.; Tatsumisago, M. High-capacity Li_2S-nanocarbon composite electrode for all-solid-state rechargeable lithium batteries. *J. Mater. Chem.* **2012**, *22*, 10015−10020.
(63) Cai, K.; Song, M.-K.; Cairns, E. J.; Zhang, Y. Nanostructured Li_2S−C Composites as Cathode Material for High-Energy Lithium/Sulfur Batteries. *Nano Lett.* **2012**, *12*, 6474−6479.

DOI: 10.1021/jp513023v
J. Phys. Chem. C 2015, 119, 4675−4683